SICE-ICASE International Joint Conference 2006
Oct. 18-21, 2006 in Bexco, Busan, Korea

Development of a Sensor System for Outdoor Service Robot

Takeshi Nishida[1], Yuji Takemura[1], Yasuhiro Fuchikawa[1], Shuichi Kurogi[1], Shuji Ito[2], Masayuki Obata[2], Norio Hiratsuka[2], Hidekazu Miyagawa[2], Yasuhiro Watanabe[3], Toshinori Suehiro[4], Yoshinori Kawamura[5] and Fujio Ohkawa[6]

[1]Faculty of Engineering, Kyushu Institute of Technology, Fukuoka, Japan
(Tel : +81-93-884-3190; E-mail: nishida@cntl.kyutech.ac.jp)
[2] YASKAWA INFORMATION SYSTEMS Corporation, Fukuoka, Japan
[3] Mechanics & Electronics Research Institute Fukuoka Industrial Technology Center, Fukuoka, Japan
[4] Fukuoka Industry, Science & Technology Foundation, Fukuoka, Japan
[5] FAIS Robotics Research Institute, Fukuoka, Japan
[6] Faculty of Computer Science and System Engineering, Kyushu Institute of Technology, Fukuoka, Japan

Abstract: The outdoor service robot, which we call OSR-02, is presently under development intended for cleaning up urban areas by means of collecting discarded trash such as plastic bottles, cans, plastic bags and so on. Additionally, we have developed a novel sensor system for the achievement of the task by this robot; it is constructed with LRF (Laser Rnagefinder), two cameras, and three stepping motors. In this paper, we describe the sensor system and its applications.

Keywords: outdoor service robot, sensor system, laser rangefinder, camera.

1. INTRODUCTION

The outdoor service robot, which we call OSR-02 (Fig.1), is presently under development intended for cleaning up urban areas by means of collecting discarded trash such as plastic bottles, cans, plastic bags and so on. Additionally, we have developed a novel sensor system which can detect the target object against the change of ambient light for the achievement of the several tasks by this robot. The sensor system consists of two kinds of sensor devices, LRF (Laser Rnagefinder) and camera; various types of measurement and detection of the target are possible according to those combinations. Moreover, this sensor system has been installed in center front of the robot as shown in Fig.1(b). In this paper, we show an application of the sensor system for trash detection and 3D posture measurement of the target after giving a briefing about the construction of the hardware.

2. STRUCTURE

2.1 Devices

The sensor system (Fig.2) consists of two cameras, a LRF, and three stepping motors. The maximum measurement distance of the LRF (URG-04LX) is 4 [m], and the measurement error margin is 1[%]. The infrared laser is radially irradiated from the center part of the LRF, its range of the measurement is forward 170 [deg] (the max range is 240 [deg]), and the angle resolution is about 0.36 [deg]. The CCD color camera captures images in 24-bit color at 640×480 resolution at rates to 30 [fps]. Moreover, these installation positions have been designed so that those optical axes and the measurement plane of LRF are parallel.

(a)

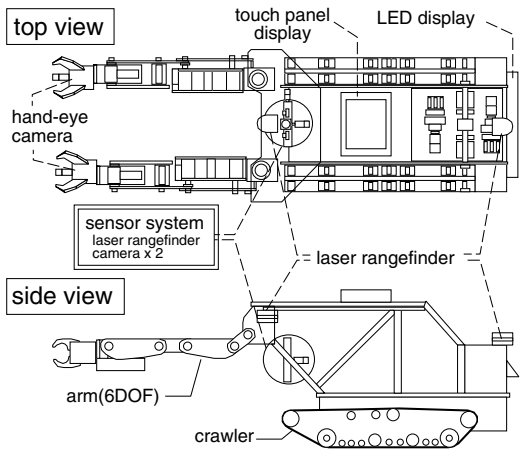

(b)

Fig. 1 Outdoor Service Robot OSR-02; (a) entire robot; (b) configuration.

This research was funded by the Robotics Industry Development Council (RIDC). The authors thank them for their support.

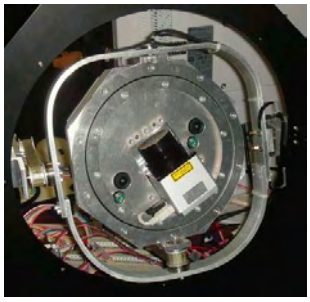

(a)

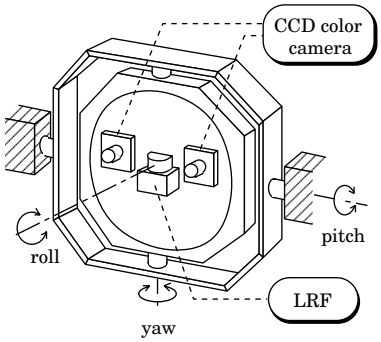

(b)

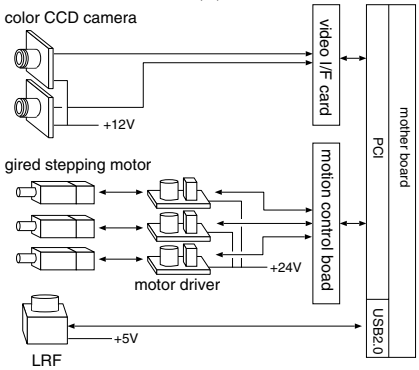

(c)

Fig. 2 Sensor system; (a) photo image; (b) structure; (c) electric structure.

Table 1 Definition of the coordinate systems.

sensor coordinate system	$\Sigma_r = \{^r x, ^r y, ^r z\}$
LRF coordinate system	$\Sigma_l = \{^l x, ^l y, ^l z\}$
left camera coordinate system	$\Sigma_{cl} = \{^{cl} x, ^{cl} y, ^{cl} z\}$
right camera coordinate system	$\Sigma_{cr} = \{^{cr} x, ^{cr} y, ^{cr} z\}$
left image coordinate system	$\Sigma_{sl} = \{^{sl} x, ^{sl} y\}$
right image coordinate system	$\Sigma_{sr} = \{^{sr} x, ^{sr} y\}$

2.2 Coordinate systems

The definition of each coordinate system and the relations between them are shown here. At first, Table 1 shows the definition of each coordinate system, and the relations between the cameras and the LRF are shown in Fig. 3. Let $\boldsymbol{R}_X(\cdot)$, $\boldsymbol{R}_Y(\cdot)$, and $\boldsymbol{R}_Z(\cdot)$ be the rotation matrix for each axis of the sensor coordinate system. The homogeneous coordinate transform matrix from the sensor coordinate system Σ_r to the LRF coordinate system

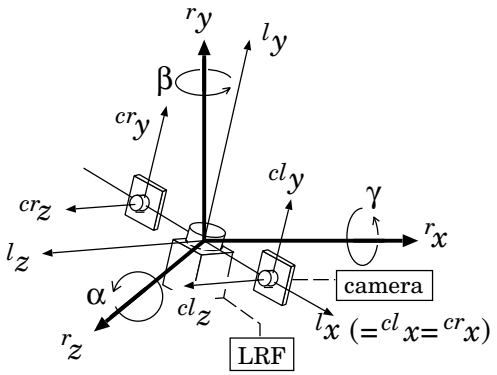

Fig. 3 Relations of coordinate systems.

Σ_l is represented as follows,

$$ {}^r_l\boldsymbol{H} \triangleq \left(\begin{array}{c|c} {}^r_l\boldsymbol{R} & {}^r_l\boldsymbol{p} \\ \hline \boldsymbol{0} & 1 \end{array} \right) \in \mathbb{R}^{4\times 4}, \tag{1} $$

where,

$$ {}^r_l\boldsymbol{R} \triangleq \boldsymbol{R}_Z(\alpha)\boldsymbol{R}_Y(\beta)\boldsymbol{R}_X(\gamma) \tag{2} $$

is the rotation matrix about angle (α, β, γ) and ${}^r_l\boldsymbol{p}$ is translate vector of the sensor coordinate system. Here, the sensor system is designed to be ${}^r_l\boldsymbol{p} \simeq \boldsymbol{0}$. Namely, the origins of Σ_l and Σ_r are overlapped and the LRF does only the gyration. From these relations, the mapping from a measurement data point ${}^l\boldsymbol{x}_{ij} \triangleq ({}^l x_{ij},\ {}^l y_{ij},\ {}^l z_{ij})^T \in \Sigma_l$ to the point ${}^r\boldsymbol{x}_{ij} \triangleq ({}^r x_{ij},\ {}^r y_{ij},\ {}^r z_{ij})^T \in \Sigma_r$ is represented by

$$ {}^r\boldsymbol{x}_{ij} = {}^l_r\boldsymbol{H} \left(\begin{array}{c} {}^l\boldsymbol{x}_{ij} \\ 1 \end{array} \right) = {}^r_l\boldsymbol{H}^{-1} \left(\begin{array}{c} {}^l\boldsymbol{x}_{ij} \\ 1 \end{array} \right), \tag{3} $$

where,

$$ {}^r_l\boldsymbol{H}^{-1} = \left(\begin{array}{c|c} {}^r_l\boldsymbol{R}^T & -{}^r_l\boldsymbol{R}^T\, {}^r_l\boldsymbol{p} \\ \hline \boldsymbol{0} & 1 \end{array} \right). \tag{4} $$

Next, the homogeneous coordinate transform matrices from the LRF coordinate system Σ_l to the left and the right camera coordinate system Σ_{cl} and Σ_{cr} are represented as follows,

$$ {}^l_{cl}\boldsymbol{H} \triangleq \left(\begin{array}{c|c} {}^l_{cl}\boldsymbol{R} & \boldsymbol{b}_l \\ \hline \boldsymbol{0} & 1 \end{array} \right), \tag{5} $$

$$ {}^l_{cr}\boldsymbol{H} \triangleq \left(\begin{array}{c|c} {}^l_{cr}\boldsymbol{R} & \boldsymbol{b}_r \\ \hline \boldsymbol{0} & 1 \end{array} \right), \tag{6} $$

where, $\boldsymbol{b}_l \triangleq (b_x, b_y, b_z)^T$ and $\boldsymbol{b}_r \triangleq (b_x, -b_y, b_z)^T$ are biases between Σ_l and Σ_{cl} (or Σ_{cr}), respectively. Therefore, the posture of the left (right) camera against Σ_r is represented by

$$ {}^r_{cl}\boldsymbol{H} = {}^r_l\boldsymbol{H}\ {}^l_{cl}\boldsymbol{H}, \tag{7} $$

$$ {}^r_{cr}\boldsymbol{H} = {}^r_l\boldsymbol{H}\ {}^l_{cr}\boldsymbol{H}. \tag{8} $$

Here, as mentioned above, the sensor system is designed to be ${}^l_{cl}\boldsymbol{R} \simeq \boldsymbol{I}$ and ${}^l_{cr}\boldsymbol{R} \simeq \boldsymbol{I}$. Next, the mapping of the LRF measurement data point ${}^r\boldsymbol{x}_{ij} \in \Sigma_l$ to the point ${}^{sl}\boldsymbol{x}_{ij}$

in the left camera image coordinate system is represented as follows,

$$
\begin{aligned}
{}^{r}_{l}\boldsymbol{R}\,({}^{r}\boldsymbol{x}_{ij} - \boldsymbol{b}_l) &\triangleq \left({}^{cl}x_{ij},\ {}^{cl}y_{ij},\ {}^{cl}z_{ij}\right)^T \\
&\triangleq {}^{cl}\boldsymbol{x}_{ij} \in \Sigma_{cl} \qquad (9)
\end{aligned}
$$

$$
\boldsymbol{f}\left({}^{cl}\boldsymbol{x}_{ij}\right) = \left(f_{cl}\frac{{}^{cl}x_{ij}}{{}^{cl}z_{ij}},\ f_{cl}\frac{{}^{cl}y_{ij}}{{}^{cl}z_{ij}}\right)^T \triangleq {}^{sl}\boldsymbol{x}_{ij}, \quad (10)
$$

where, f_l is the focal length of the left camera. Moreover, the mapping from the point ${}^{sl}\boldsymbol{x}_{ij}$ to the pixel on the left camera screan is as follows,

$$
F({}^{sr}\boldsymbol{x}_{ij}) = \begin{pmatrix} s_x \cdot {}^{sr}x_{ij} \\ s_y \cdot {}^{sr}y_{ij} \end{pmatrix} \triangleq {}^{sr}\boldsymbol{x}_{mn}, \qquad (11)
$$

where, $M = \{m|1, \cdots, |M|\}$! $N = \{n|1, \cdots, |N|\}$ are width and height indexes of pixel on an image. Hence, the measurement data points of the LRF are mapped into the left camera screen pixels by Eqn. (9), (10), (11).

The measurement data between devices is mutually mapped by the above relational expressions.

2.3 Target detection and measurement

The detection and the tracking of the target object by the camera image processing are influenced easily from the change in ambient light while it is comparatively high-speed executable. The calculation cost for the measurement and the detection of the object by the LRF is comparatively high, however, the measurement is robust under the influence of ambient light. Therefore, the sensor system with the cameras and the LRF can execute various types of measurement robust to the change of the environment. For example, the measurement data sets of each device are combined to complement each other for high accuracy detection and measurement. Otherwise, a limited measurement for fast computation is possible by only one device. In this research, we employ the image processing method for detection and tracking of the object developed on the assumption of installing in the robot. For fast computation in this image processing, we employ the eigen space method for pattern matching [1] and the CAMSHIFT algorithm [2] for target tracking (see [3] for detail). Moreover, we employ the PSF (Plane Segment Finder) method, which appears below, to analyze of the range data. The flowchart of an application of the sensor system is shown in Fig. 4. In this application, at first, a target object is detected and tracked by camera image processing, and after that, the range data of the object obtained by rotating the LRF is analyzed. By a such measurement flow, the object detection is quickly achieved by the camera image processing, and the analysis in detail of the target object is done by using the LRF data not influenced easily from an environmental change.

3. RANGE DATA EXTRACTION

It is necessary to extract the data set of the target object from the measurement data set for the analysis of the object. Therefore, in this research, we employ the PSF (Plane Segment Finder) method [4] using Randomized

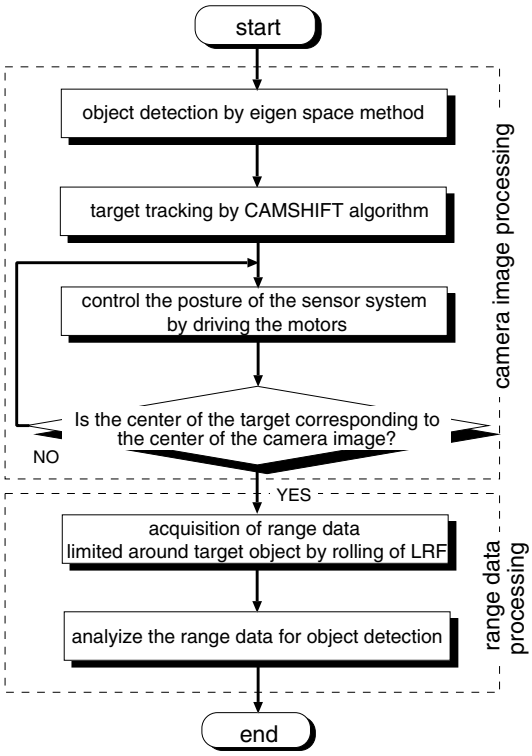

Fig. 4 Flowchart of an application of the sensor system.

Hough Transform [5] to extract the plane such as the surface the floor and so on from the range data set. A concrete procedure is shown as follows.

First, let ${}^{r}\boldsymbol{x}_{ij} \triangleq ({}^{r}x_{ij},\ {}^{r}y_{ij},\ {}^{r}z_{ij})^T$ $(i = 1, \cdots, |I|)$, $(j = 1, \cdots, |J|)$ be the measurement points (Fig. 5). Next, $\theta_{ij} (0 \leq \theta_{ij} < \pi)$ and $\phi_{ij} (0 \leq \phi_{ij} < \pi)$ (Fig. 6) are calculated from the normal vector of the plane including the points $(\boldsymbol{x}_{ij}, \boldsymbol{x}_{i+s,j}, \boldsymbol{x}_{i,j+s})$ as follows,

$$
\begin{aligned}
\theta_{ij} &= \tan^{-1}\left(n^y_{ij}/n^x_{ij}\right), \qquad (12) \\
\phi_{ij} &= \tan^{-1}\left({n^z_{ij}}^2 / \left({n^x_{ij}}^2 + {n^y_{ij}}^2\right)\right)^{\frac{1}{2}}, \qquad (13)
\end{aligned}
$$

where,

$$
\begin{aligned}
\boldsymbol{n}_{ij} &= \frac{\boldsymbol{l}_{ij} \times \boldsymbol{m}_{ij}}{|\boldsymbol{l}_{ij} \times \boldsymbol{m}_{ij}|} \triangleq (n^x_{ij}, n^y_{ij}, n^z_{ij})^T, \qquad (14) \\
\boldsymbol{l}_{ij} &= \boldsymbol{x}_{i+s,j} - \boldsymbol{x}_{ij}, \qquad (15) \\
\boldsymbol{m}_{ij} &= \boldsymbol{x}_{i,j+s} - \boldsymbol{x}_{ij}, \qquad (16)
\end{aligned}
$$

and s represents an interval of index of data point. The peak cells of (θ_{ij}, ϕ_{ij}) in θ-ϕ space are searched. The values of points around the found peak are replaced with the value of the peak (θ', ϕ'), and the following values are calculated.

$$
\rho'_{ij} = (x_{ij}\cos\theta' + y_{ij}\sin\theta')\cos\phi' + z_{ij}\sin\phi'. \quad (17)
$$

The peak value $\bar{\rho}'$ of ρ'_{ij} is searched. The data points with the distance values ρ'_{ij} close to the peak value $\bar{\rho}'$ are estimated to be existence on the same plane. Therefore, these data points estimated that they are in a plane surface are extracted from the range data set.

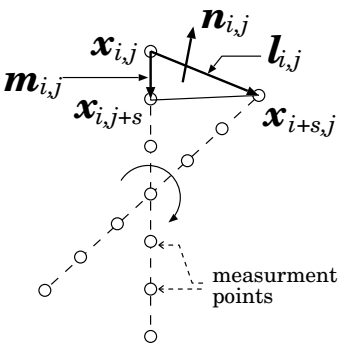

Fig. 5 Relations of the measurement points.

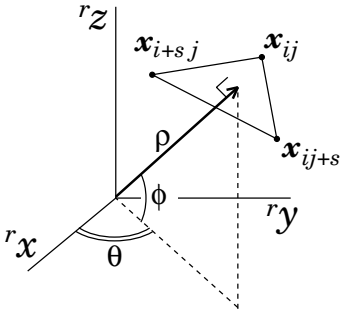

Fig. 6 Relations of the coordinate system and Hough parameters.

4. EXPERIMENT

We conducted the experiment that detected and measured a plastic bottle by the sensor system and evaluated the system.

4.1 Target detection and tracking by image processing

A plastic bottle was put in front of the sensor system, and the detection and the measurement sequences of the sensor system were evaluated. The example of the result of the camera image processing is shown in Fig. 7. We see from that the motors of the sensor system were controlled appropriately to track the object detected by the camera image processing. Moreover, it was confirmed that the distance to the object, the position, and posture information etc. of the target object were calculated in real time (30 [fps]).

4.2 Object measurement by LRF

Fig. 8 shows the measurement range data of the target object. As the figure indicates, only the surrounding of the target is measured in high density by the rolling of the LRF. Next, to extract and remove the floor surface from this measurement data, the above mentioned PSF method was applied to this data according to the following procedures. At first, we set $s = 2$ and calculate normal vectors $\boldsymbol{n}_{ij}$ (Fig. 9(a)). We see from this figure that the normal vectors were distributed around $\boldsymbol{n}_{ij} = (0, 1.0, 0)^T$ but the specification of the peak of the distribution is difficult. Next, the values of $(\theta_{ij}, \phi_{ij}, \rho_{ij})$ in Hough space were calculated from these normal vectors, and they plotted in the graph shown in Fig. 9(b). Here, the values of

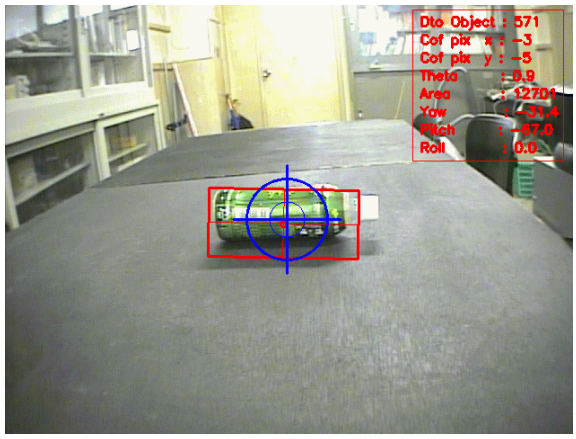

Fig. 7 Example of the detection and the measure of a plastic bottle. The scope mark shows the center of the image, and the square around the plastic bottle shows the range where the detected object exists.

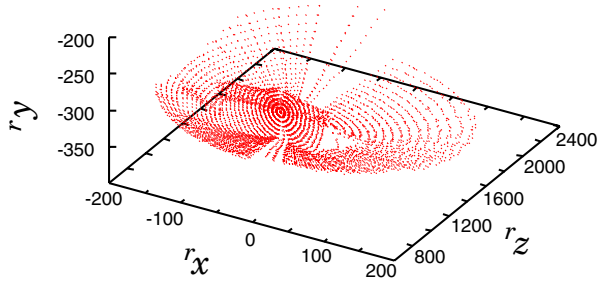

Fig. 8 The range data set of the detected plastic bottle.

ρ_{ij} were obtained by the following expression.

$$\rho_{ij} = (x_{ij}\cos\theta_{ij} + y_{ij}\sin\theta_{ij})\cos\phi_{ij} + z_{ij}\sin\phi_{ij} \quad (18)$$

Since the variance of ρ_{ij} caused by the measurement noise were large relatively, it is also difficult to specify the peak of the plot point from this graph. Therefore, the values of (θ_{ij}, ϕ_{ij}) were normalized and mapped into $\bar{\theta}$-$\bar{\phi}$ space and two dimension histogram of 36×36 division was generated (Fig. 9(c)). It is found that the peak exists at $(90, 0)$ from this figure. Next, we set $(\theta', \phi') = (90, 0)$, the values ρ'_{ij} were calculated as shown in Eqn. (18), and separate the range data based on the threshold $\rho'_{ij} \geq 300$ [mm]. This threshold value was set referring to local minimum value of the distribution. The separated range data of the floor surface is shown in Fig. 11(a), and the left range data is shown in Fig. 11(b). We see from these results that the floor surface was separated from the measurement range data set, and the target object was able to be extracted. However, we also see from Fig. 11(b) that the other range data points were left around the data of the target, and the elimination of these data points is a future work. Moreover, the object recognition of the target that uses the extracted range data set is a future work.

5. CONCLUDING REMARKS

In this research, the novel sensor system and its applications for the mobile robot has been proposed and

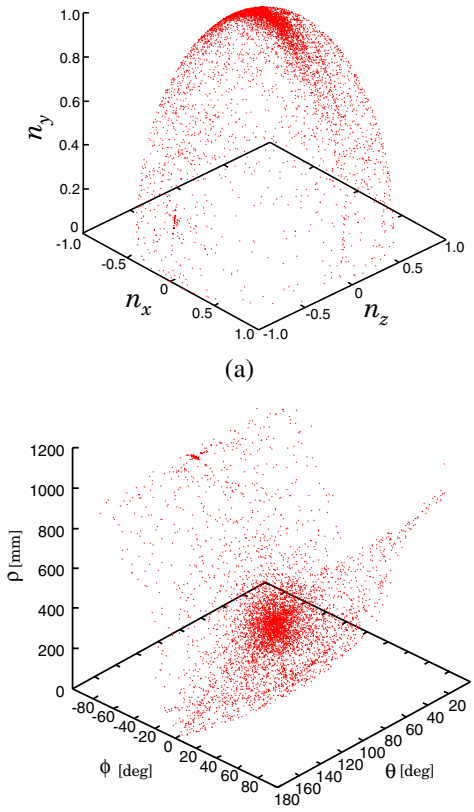

(a)

(b)

Fig. 9 Distribution of vectors; (a) normal vectors; (b) $(\rho_{ij}, \theta_{ij}, \phi_{ij})$ vectors calculated from the range data set.

constructed, and its effectiveness is shown by the experiments. Various processing by correspondence the measurement data of the camera and the LRF installed into the sensor system as shown in this paper is possible, and it is developing now.

REFERENCES

[1] M. Uenohara and T. Kanade, "Use of Fourier and Karhunen-Loeve Decomposition for Fast Pattern Matching With a Large Set of Templates," *IEEE trans. on pattern analysis and machine intelligence*, vol. 19, no. 8, pp. 891–898, 1997.

[2] Gray R. Bradski, "Computer vision face tracking as a component of a perceptual user interface", *In Workshop on Applications of Computer Vision*, pp. 214–219, 1998.

[3] Y. Fuchikawa, T. Nishida, S. Kurogi, T. Kondo, F. Ohkawa, T. Suehiro, Y. Watanabe, Y. Kawamura, M. Obata, H. Miyagawa and Y. Kihara, "Development of a Vision System for an Outdoor Service Robot to Collect Trash on Streets," *Proc. of CGIM05*, pp.100-105, 2005.

[4] K. Okada, S. Kagami, M. Inaba, H. Inoue, "Plane Segment Finder: Algorithm, Implementation and Applications", *Proc. of Int. Conf. on Robotics and Automation*, pp. 2120-2125, 2001.

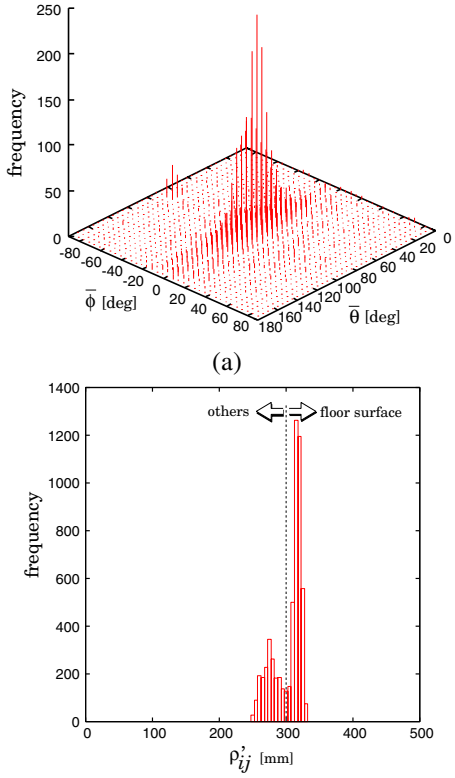

(a)

(b)

Fig. 10 Histgram of (a) normarized Hough parameter and of (b) ρ'_{ij}.

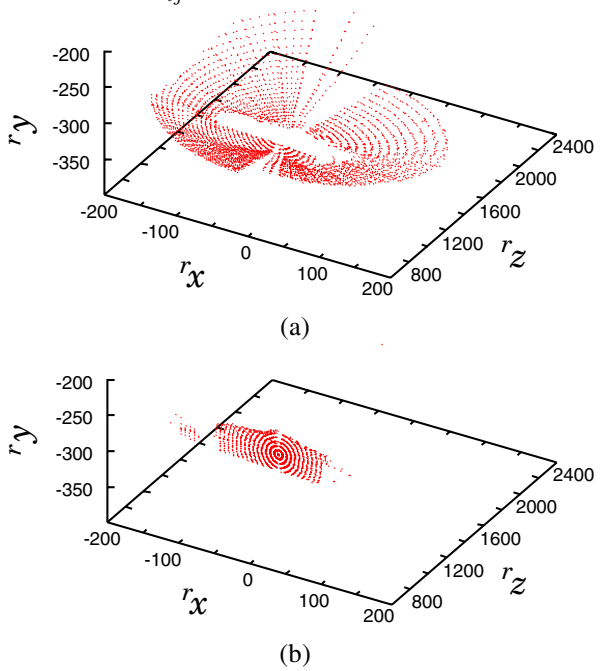

(a)

(b)

Fig. 11 Example of the detection and the measure of a plastic bottle; (a) result of extraction of the floor surface, and (b) range data set of the plastic bottle.

[5] Y. Ding, X. Ping, M. Hu and D. Wang, "Range Image Segmentation Based on Randomized Hough Transform", *Pattern Recognition Letters*, no. 26, pp. 2033-2041, 2005.